



# CHORUS

This is the accepted manuscript made available via CHORUS. The article has been published as:

## Intrinsic dynamics of the electric-field-induced phase switching in antiferroelectric $\text{PbZrO}_3$ ultrathin films

Z. G. Fthenakis and I. Ponomareva

Phys. Rev. B **98**, 054107 — Published 21 August 2018

DOI: [10.1103/PhysRevB.98.054107](https://doi.org/10.1103/PhysRevB.98.054107)

# Intrinsic dynamics of the electric-field-induced phase switching in antiferroelectric $\text{PbZrO}_3$ ultrathin films

Z. G. Fthenakis<sup>1</sup> and I. Ponomareva<sup>1</sup>

<sup>1</sup>*Department of Physics, University of South Florida, Tampa, Florida 33620, USA*

## Abstract

Antiferroelectric ultrathin  $\text{PbZrO}_3$  films can exhibit both ferroelectric and antiferroelectric behavior depending on the thickness. We use first-principles-based nanoscopic simulations to investigate the intrinsic high-frequency dynamics of the electric-field-induced phase switching in such films which so far remains unknown. In this comprehensive study we report i) the size and frequency evolution of the polarization response to the electric field; ii) the intrinsic time for the phase switching; iii) detailed comparison between the polarization reversal in the films with ferroelectric and antiferroelectric behavior; (iv) dynamics of the antiferroelectric and antiferrodistortive order parameters; (v) nanoscopic mechanism responsible for the phase switching. The nanoscopic insight leads to the prediction of the existence of two possible scenarios for the antipolar-polar phase switching depending on the mutual orientation of the antiferroelectric order parameter and the electric field. The two scenarios have different dynamical fingerprints. The polar-antipolar phase switching is found to be assisted by the formation of a nonpolar phase. Computational data indicate that the phase switching time is only fractions of nanoseconds for the polar-polar phase switching in ferroelectric films and polar-antipolar phase switching in antiferroelectric films. The antipolar-polar phase switching in antiferroelectric films is just a bit slower and takes the order of nanosecond. Under nonequilibrium conditions we find formation of antiferroelectric and antiferrodistortive nanodomains and coexistence of polar and antipolar order parameters.

## INTRODUCTION

Antiferroelectric (AFE) thin films are the antipolar counterparts of the ferroelectric (FE) thin films. They exhibit high-energy storage densities and fast discharge times in capacitors [1], unusual electrocaloric properties [2, 3], strong dependence of the electric properties on the film's orientation, composition, and large nonlinear electromechanical response [4]. They allow integration with silicon technology and could be used in high energy storage capacitors, micro-actuators, pyroelectric security sensors, cooling devices, pulsed power generators and others [4]. The most attractive feature of the AFE thin films is the energetic proximity of the polar and antipolar phases which allows the phase control by the application of external electric field. As a result, the field-induced phase transitions in AFE bulk and thin films is under intense investigation [4]. At the same time, to the best of our knowledge, no studies have been carried out on ultrathin AFE films subjected to high frequency electric fields. Ultrathin AFE films, unlike their FE counterparts, are only beginning to reveal their unique properties and technological potential. For example, it was predicted computationally that AFE  $\text{PbZrO}_3$  films exhibit a size-driven transition into a FE behavior below the critical thickness of 15 unit cells [5, 6]. Experimentally, AFE  $\text{PbZrO}_3$  films were synthesized down to thicknesses of 11 unit cell and were found to exhibit both AFE behavior in their virgin state and FE behavior after repetitive cycling of the electric field [7]. Moreover, this pioneering study unveiled the potential of such films to function as unusual tunnel junctions. AFE ultrathin layers of  $\text{PbZrO}_3$ , were also reported to contribute to the unusual properties of AFE/FE superlattices [8, 9]. At the same time, the nanoscopic insight into the electric-field-induced phase transition in such ultrathin films is presently missing. The macroscopic model of the phase switching in antiferroelectrics proposed by Park [10] is based on six stages and involves AFE domains. At the same time the model is unlikely to be applicable for ultrathin films which cannot develop macroscopic domains. Does the mechanism involve formation and propagation of nanoscale domains or is it replaced with homogeneous phase transition similar to the case of FE ultrathin films and nanostructures [11–13]? Furthermore, the kinetics of the polar-antipolar phase transition at the nanoscale is presently unknown. What are the intrinsic time(s) associated with the phase switching? How do the electric properties change as the period of the electric field approaches this characteristic time scale? In addition, the dynamics of the other order parameters, such as AFE and antiferrodistortive

(AFD) order parameters, is also unknown. As scientific curiosity and technological needs drive the fundamental and applied research to ever shrinking size and time scales the question about high frequency dynamics in AFE ultrathin films becomes of paramount importance.

In the computational study of Ref. 14 the polarization switching in a hypothetical two-dimensional antiferroelectric was investigated. A single characteristic time for the polarization switching was found. The frequency evolution of the hysteresis loops was explored in details. With the increase in frequency the characteristic AFE double loops were transitioning into broader oval-like shapes. The evolution was found to be dependent on the amplitude of the driving field. However, the two-dimensional model and quasi-static nature of the simulations pose severe limitations on the computational predictions. In particular, the dipole orientation and dynamics as well as the electric field direction are restricted to the plane, which excludes alternative routes for the phase transitions, such as through the out-of-plane dipole rotations. A number of studies have been carried out on different aspects of the dynamics of antiferroelectrics in bulk and film forms typically for the electric field frequency up to 10 kHz [15–19]. A scaling behavior for the area of hysteresis loops in AFE betaine phosphatearsenate ( $\text{BP}_{0.9}\text{A}_{0.1}$ ) crystal was observed below the frequency of 200 Hz [15]. A scaling behavior of energy storage density on the frequency in the range of 1 to 100 Hz was reported in AFE  $\text{Pb}_{0.99}\text{Nb}_{0.02}[(\text{Zr}_{0.60}\text{Sn}_{0.40})_{0.95}\text{Ti}_{0.05}]\text{O}_3$  ceramics [16]. Kinetics of the polarization switching in AFE thick  $\text{Pb}_{0.97}\text{La}_{0.02}(\text{Zr}_{0.95}\text{Ti}_{0.05})\text{O}_3$  films was experimentally investigated under an applied electric field with frequency ranging from 2 Hz to 10 kHz [17]. Only very weak dependence on frequency was found and a characteristic switching time of  $\sim 3$  ns was inferred on the basis of the nucleation-limited-switching theory. The charge release time of 6 ns was reported for AFE  $0.4 \mu\text{m}$   $\text{Pb}_{0.97}\text{La}_{0.02}(\text{Zr}_{0.85}\text{Sn}_{0.13}\text{Ti}_{0.02})\text{O}_3$  films [18]. In AFE ceramics a difference between the quasi-static (100 Hz) and dynamic (pulsed current) hysteresis loops were reported under an applied electric field of 36 kV/cm [19]. At the same time, no studies on the dynamics of the AFE *ultrathin* films under *high* frequency electric field are available, to the best of our knowledge. So the aim of this Paper is to report room temperature intrinsic high-frequency (GHz and above) dynamics of the AFE  $\text{PbZrO}_3$  films ranging in thickness from 10 to 20 unit cells. More specifically we report: i) the nanoscopic mechanism responsible for the electric-field-induced phase transitions in such films; ii) the evolution of the hysteresis loops as a function of the electric field frequency; iii) the dynamics of the AFE and AFD order parameters; iv) the changes in the dynamics that

occur with the decrease in film's thickness; v) intrinsic phase switching times in such films.

## METHODOLOGY

To achieve our aim we simulate room temperature high-frequency dynamics of  $\text{PbZrO}_3$  ultrathin films ranging in thickness from 10 to 20 unit cells grown along [001] crystallographic direction. These films, model experimentally synthesized  $\text{PbZrO}_3$  films [7]. The films are simulated by  $16 \times 16 \times N$  supercell with periodic boundary conditions applied along the in-plane directions (x- and y-Cartesian axes in our setup). Along the out-of-plane direction (z-Cartesian axis in our setup) the number of unit cells,  $N$ , corresponds to the thickness of the film. The energy of the supercell is given by the first-principles-based effective Hamiltonian of Ref. 20. The degrees of freedom for the effective Hamiltonian include polar local modes,  $\mathbf{u}_i$ , which are proportional to the local dipole moment in the unit cell  $i$  and describe the AFE instability at  $\Sigma_2$  point of the Brillouin zone, AFD local modes,  $\mathbf{w}_i$ , that describe oxygen octahedra tilts about Cartesian axes and are responsible for the  $R_4$  point instability, and inhomogeneous and homogeneous strain variables, which describe elastic deformations of the unit cell and supercell, respectively. The Hamiltonian includes energy associated with the AFE  $\Sigma_2$  mode and contains contributions from the dipole-dipole interactions, short-range interactions, and on-site self-energy. It also includes energy due to the AFD mode that is similar to the previous one but excludes the dipole-dipole interactions as AFD local modes are nonpolar. Finally, the Hamiltonian includes the energy associated with elastic deformations. All degrees of freedom are coupled with each other by the symmetry allowed interactions. Simulation of an external electric field is achieved by adding a term to the effective Hamiltonian that couples electric dipoles with the electric field. All parameters of the effective Hamiltonian are derived from the local-density-approximation-based density functional theory calculations [20]. This Hamiltonian correctly reproduces the sequence of phase transition in  $\text{PbZrO}_3$ , its electrical properties and behavior under pressure [20]. The following modifications to the effective Hamiltonian for bulk  $\text{PbZrO}_3$  are used to simulate thin films. i) Periodic boundary conditions are applied along the in-plane directions only using the computational approach of Ref. 21. ii) The macroscopic depolarizing field is screened by introducing a screening term in the effective Hamiltonian [21]. The screening term describes the interaction of the local modes with the macroscopic electric field that

opposes the depolarizing field and has the magnitude  $\beta E_{dep}^{max}$ , where  $E_{dep}^{max}$  is the maximum depolarizing field associated with the given dipole configuration. The screening parameter  $\beta$  can take values from 1 to 0, which correspond to the ideal short-circuit and open-circuit boundary conditions, respectively. The surface charge compensation was previously found to critically affect phases in  $\text{PbZrO}_3$  nanostructures [6]. For this study we use  $\beta$  of 0.98 to model films with very good but yet realistic surface charge compensation. In order to study intrinsic dynamics of such films we simulate stress-free mechanical boundary conditions.

The effective Hamiltonian is used in the framework of classical Molecular Dynamics (MD) with the Newton equations of motion integrated for all degrees of freedom using a predictor-corrector algorithm [22]. The integration step was set to 1 fs. To simulate constant temperature conditions we used the Evans-Hoover thermostat [22]. Previously such methodology was applied to study the intrinsic dynamics of  $\text{PbZrO}_3$  bulk and the computational results were found to agree with the experimental data [23]. To obtain equilibrium configurations the supercells were annealed from 1500 K down to 5 K in steps of 5 K. For each temperature we used 10000 MD steps. To study room temperature high-frequency dynamics of the field-induced phase transition we apply an ac electric field along the film's growth direction. The frequency of the field ranged from 0.001 THz to 5 THz. In particular we performed simulations for the frequencies  $\nu = 0.001, 0.002, 0.005, 0.01, 0.02, 0.05, 0.1, 0.2, 0.5, 1, 2$  and 5 THz, which are nearly equidistant on a logarithmic scale. For  $\nu < 0.001$  THz we do not expect significant differences compared to the quasi-static case. The field amplitude was set to 4.0 MV/cm which is much larger than the computational coercive field of 2.5 MV/cm in bulk  $\text{PbZrO}_3$  [20]. Computational coercive field in ultrathin  $\text{PbZrO}_3$  films is 1-2 MV/cm [6]. Thus, qualitatively, the amplitude of the applied field in this study is about twice the coercive field under quasi-static field application. The computational coercive fields overestimate the experimental values in  $\text{PbZrO}_3$  and  $\text{PbZrO}_3$ -derived compounds that range from 0.04 to 0.6 MV/cm [1, 16, 17, 24] which is partly due to the defect-free nature of the simulated samples and partly due to the force field for  $\text{PbZrO}_3$  [20]. Experimentally, fields up to 1.9 MV/cm were applied to  $\text{Pb}_{0.97}\text{La}_{0.02}(\text{Zr}_{0.95}\text{Ti}_{0.05})\text{O}_3$  AFE thick films [17]. The total simulation time for each simulation was between 0.04 and 10 ns, depending on the frequency of the electric field. For the lower frequency simulations ( $\nu < 1$  THz) we model 10-30 periods of the ac electric field, while for the higher frequencies ( $\nu \geq 1$  THz) we model 40-200 periods. During the field application the response of the polarization, AFE and AFD

order parameter is collected. We have also performed some quasi-static simulations using Metropolis Monte Carlo algorithm.

## DYNAMICS OF THE PHASE SWITCHING AND POLARIZATION REVERSAL

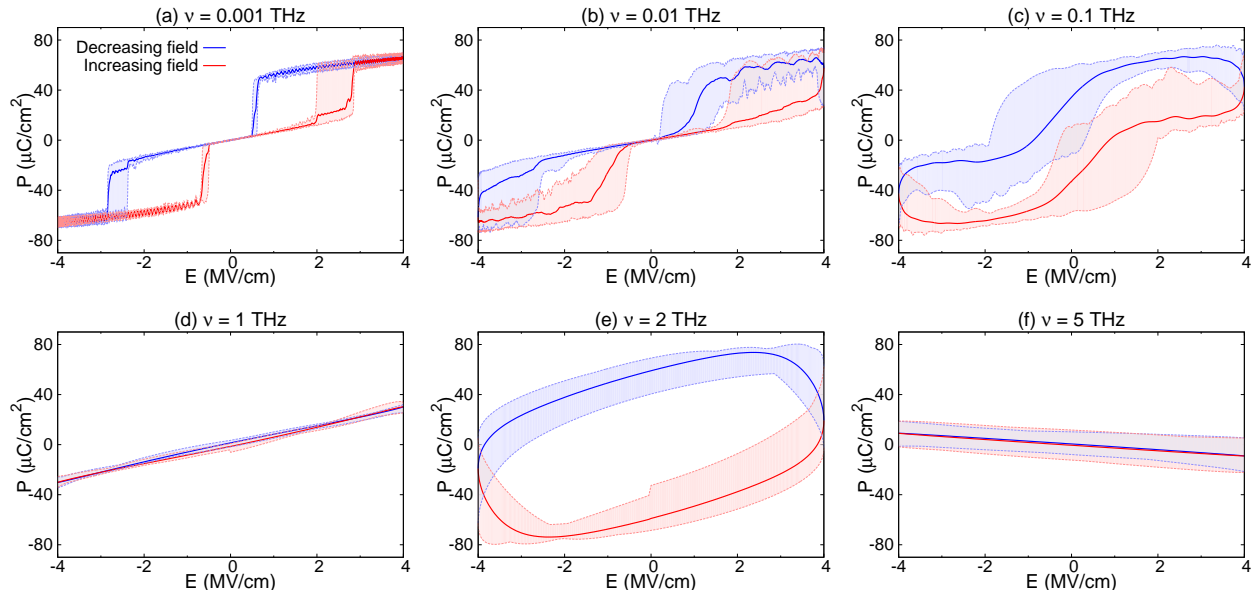


FIG. 1. Electric field evolution of polarization in the 19 unit cell thick film subjected to the electric field with the frequencies listed in the titles. The solid lines give data averaged over all periods, while shaded areas give the largest deviations from the average.

We begin with the investigation of the room temperature phase switching and polarization reversal dynamics in  $\text{PbZrO}_3$  films. It has been previously reported that AFE  $\text{PbZrO}_3$  ultrathin films exhibit FE behavior below the critical thickness of 15 unit cells under the condition that the surface charge associated with the polarization discontinuity is well compensated [5]. Note, that this is in a qualitative agreement with the experimental finding that ultrathin  $\text{PbZrO}_3$  films exhibit both FE and AFE behavior [7]. According to the computational predictions of Ref. 5 and findings of this work under the dc electric field the films with the thickness below 5.0 nm exhibit single loop structures typical of FE behavior (see Fig. 3(a) for an example). For thicknesses of 6.2 nm and above they exhibit double loop structures typical of AFE behavior (see Fig. 1(a) for an example). For the thicknesses in between 5.0 and 6.2 nm they exhibit the so-called “mixed” loops where the double loop structure coexists with spontaneous polarization (see Fig. 2(a) for an example). This is in

qualitative agreement with experimental findings [25]. The origin of this behavior was traced to the stabilization of the FE phase by the surface effects [5]. In particular, the presence of the surface eliminates energetically costly head-to-tail dipoles, thus favoring the FE phase. We expect, therefore, that the dynamics of the phase switching and polarization reversal will depend strongly on the film's thickness.

We begin the discussion with the 19 unit cell thick film that exhibits AFE behavior under quasi-static electric field [5, 7]. The field evolution of the polarization,  $P$ , averaged over all simulated periods is given in Fig. 1. Different panels display data for different frequencies of the electric field,  $E$ . The shaded areas indicate largest deviations from the average. Fig. 1(a) shows that for the lowest investigated frequency of 0.001 THz the film is AFE as evident from the double loop structure of the  $P(E)$  and zero spontaneous polarization. At the same time, there exist some deviations from the average which suggest that in this case the period of the electric field is close to the intrinsic switching time between the antipolar and polar phases. Note, that the switching time here is dominated by the waiting time for the nucleation in terms of the nucleation-limited-switching model [26]. Quantitatively, this puts the intrinsic phase switching time into ns range which compares well with the experimental values of 3 and 6 ns [17, 18]. Interestingly, the deviations are mostly limited to the variations in the coercive field for the antipolar-polar phase switching, which indicates that this phase transition is a bit slower than its polar-antipolar counterpart, which is in agreement with the experimental findings [19]. Overall, the onset of dynamical features do not change the character of the hysteresis loop. As the frequency is doubled, the variations with respect to the average increase but are still limited to the antipolar-polar phase switching. Further increase of frequency to 0.005 THz value leads to much larger deviations from the average behavior which now affects coercive fields for both antipolar-polar and polar-antipolar phase switching along with the values of saturation polarization. This puts the intrinsic switching time for the polar-antipolar phase transition into fraction of nanosecond time scale.

For frequency of 0.01 THz [Fig. 1(b)] the variations between the hysteresis loops from different periods are quite large which indicates that the one sweep of electric field (equivalent to a quarter period) is now smaller than the intrinsic phase switching time. Indeed, we can see that the average loops now do not reach saturation which suggests that the antipolar phase lingers longer than the forward sweep of the electric field. Further increase in frequency by an order of magnitude leads to the dramatic change in the appearance of the hysteresis

loops (Fig. 1(c)). The average loops do not saturate and exhibit “remnant” polarization. The variations (see shaded areas) indicate that during some periods the film exhibits “remnant” polarization as the change in the electric field occurs faster than the time required to switch the phase.

Further order of magnitude increase in frequency [Fig. 1(d)] leads to the disappearance of the hysteresis and variations between different periods of the electric field. Clearly in this case the field changes faster than the time required to complete the switching between the antipolar and polar phases. The film’s response to the electric field is governed by the response of the polar phonon. For frequency 2 THz [Fig. 1(e)] the  $P(E)$  dependence undergoes yet another dramatic transformation. This one is due to the onset of the dielectric losses associated with polar phonon mode. The increase in polarization as compared to the case shown in Fig. 1(d) is associated with the increase in the real part of the dielectric susceptibility, while the shape change of the loop is governed by increase in the imaginary part of the dielectric susceptibility which describes the lag of the polarization behind the electric field. Note, that in Ref. 23 the intrinsic frequency of the polar mode in bulk  $\text{PbZrO}_3$  was found to be in 2.4 – 4.2 THz range. Further increase in the frequency to 5 THz results in the change of sign of the slope for  $P(E)$  as the real part of the dielectric susceptibility becomes negative causing the dipoles to respond to the electric field in antiphase. We find similar features of the loops for the films with 16, 17 and 18 unit cell thickness.

The films with the thicknesses 13-15 unit cells show “mixed” hysteresis loops at the lowest frequency, where the double loop structure coexists with the spontaneous polarization [see Fig. 2(a)]. The polar and antipolar phases are extremely close in energy in this thickness range [5]. Fig. 2 shows the room temperature hysteresis loops for different frequencies for the film of 14 unit cells thickness. Dynamics of the polarization reversal in these films shows features somewhat similar to the previously described case. There exist the following differences. i) For 0.01 THz frequency the polarization reaches saturation which we attribute to the fact that the two phases are very close in energy. ii) For frequency 1 THz we now find lossy behavior which is likely to originate from the contributions from the FE phase. Interestingly, for the frequencies in the range between 0.01 and 0.1 THz, we find that during some periods the film exhibits AFE behavior, while for others it exhibits FE behavior. This is evident from the change of the character of the loops on going from frequency 0.001 THz to 0.01 THz. This is a dynamical signature of the FE-AFE phase competition, which is

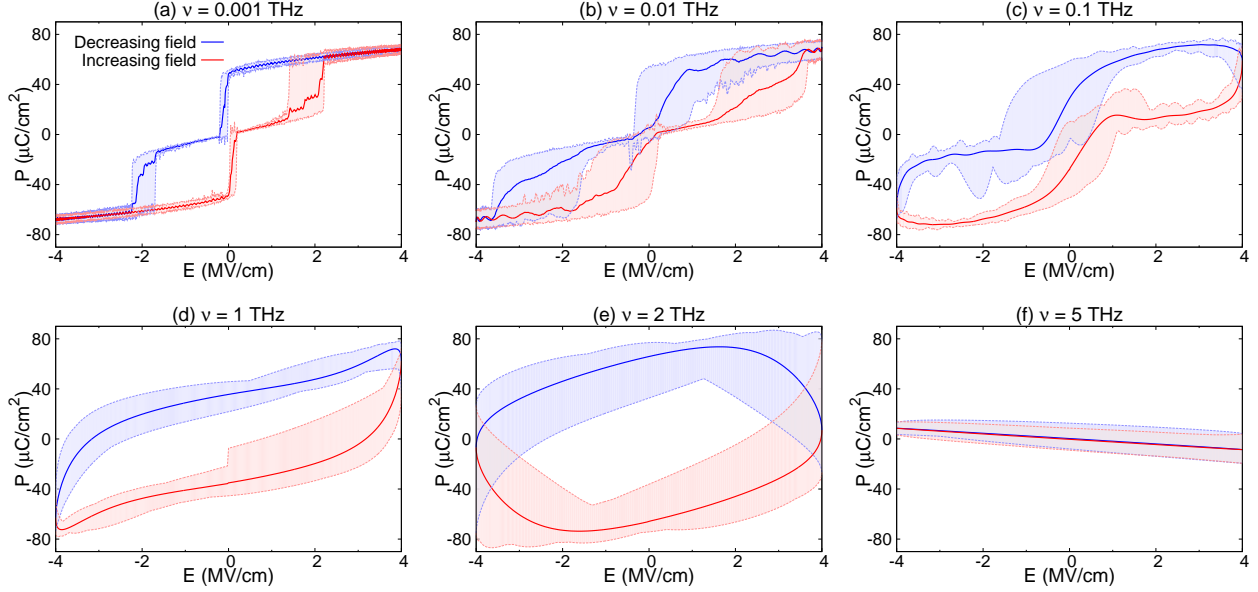


FIG. 2. Electric field evolution of polarization in the 14 unit cell thick film subjected to the electric field with the frequencies listed in the titles. The solid lines give data averaged over all periods, while shaded areas give the largest deviations from the average.

consistent with the experimental findings of Ref. 7.

Films with thicknesses 10, 11 and 12 unit cells exhibit FE behavior under quasi-static electric field [5]. Fig. 3 shows computational data for  $P(E)$  for the 11 unit cell thick film. For the lowest frequency of 0.001 THz the film exhibits FE behavior with negligible deviations from the average  $P(E)$ . As the frequency is doubled these deviations increase slightly, while for frequency 0.005 THz the deviations are quite large, indicating that now the sweep of an electric field period is comparable to the intrinsic polarization reversal time in ferroelectric ultrathin films. Qualitatively, we find that this time is shorter than the time required for the antipolar-polar phase switching, which is in agreement with experimental findings [17]. The data for 0.01 and 0.1 THz are given in Fig. 3(b) and (c). For these frequencies we find that the film can exhibit FE, AFE or “mixed” behavior at different periods. This results in the change of the shape of the loop from typical FE to a double loop AFE structure with remnant polarization. Such shape is in qualitative agreement with experimental loops [24]. For the frequencies 0.1 THz and above the behavior is similar to the previously considered case of 14 unit cells thick film.

To gain further insight into the intrinsic dynamics of the field induced phase switching we plot the average energy loss per electric field period as a function of the electric field frequency

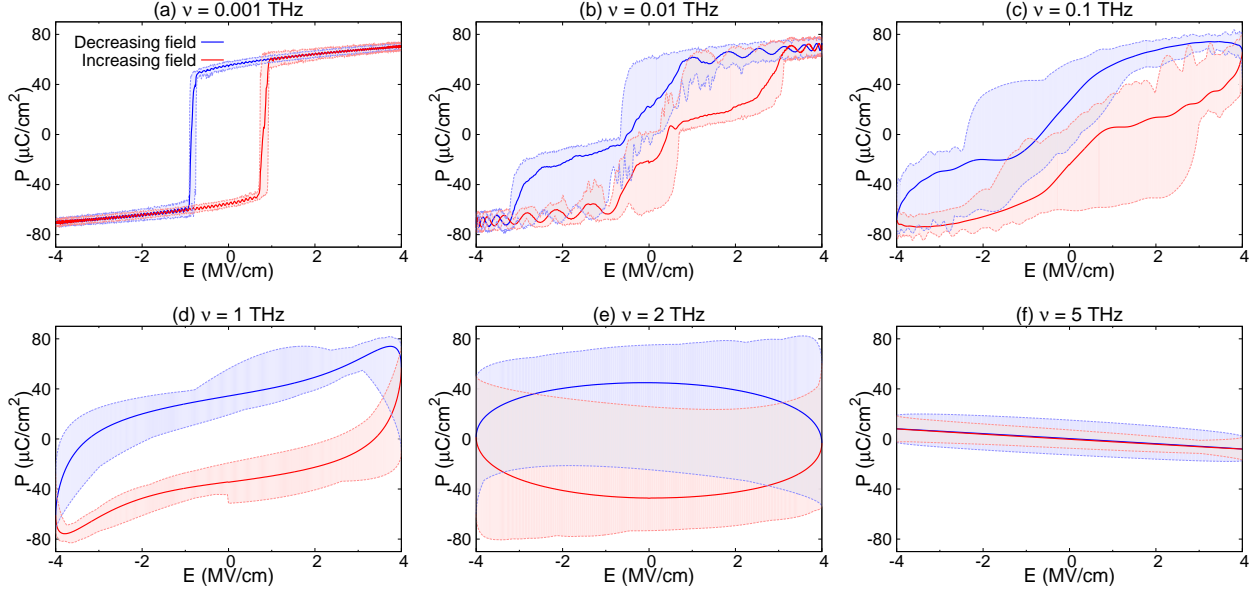


FIG. 3. Electric field evolution of polarization in the 11 unit cell thick film subjected to the electric field with the frequencies listed in the titles. The solid lines give data averaged over all periods, while shaded areas give the largest deviations from the average.

for 11 and 19 unit cell thick films (representatives of the FE and AFE behavior, respectively) in Fig. 4. The shaded area indicates the largest deviation from the average. For both films we notice that at the lowest frequency the deviations are rather small, especially for the FE film. As the frequency increases both the deviations and the average value increase indicating that the frequency is now close to the frequency of the intrinsic switching dynamics. For the FE film the largest losses and deviations are in the 0.2-2 THz range where the losses due to the dynamics of the phase switching overlap with the losses due to the intrinsic polar mode dynamics (2.4 - 4.2 THz frequency range in bulk [23]). For the AFE film the losses are nearly zero in the same frequency range as the film exhibits linear dielectric behavior in this range [see Fig. 1(d)]. These suggest that below 0.2 THz the dynamics is dominated by the kinetics of the phase switching, while for higher frequencies polar phonon dynamics contributes as well. The peak in losses occurs at 2 THz and is associated with the losses due to intrinsic polar mode dynamics. For the lowest frequency the deviations from the average value are smaller in the FE film as compared to the AFE film, which further suggests that the polarization reversal time is indeed shorter than the antipolar-polar switching time.

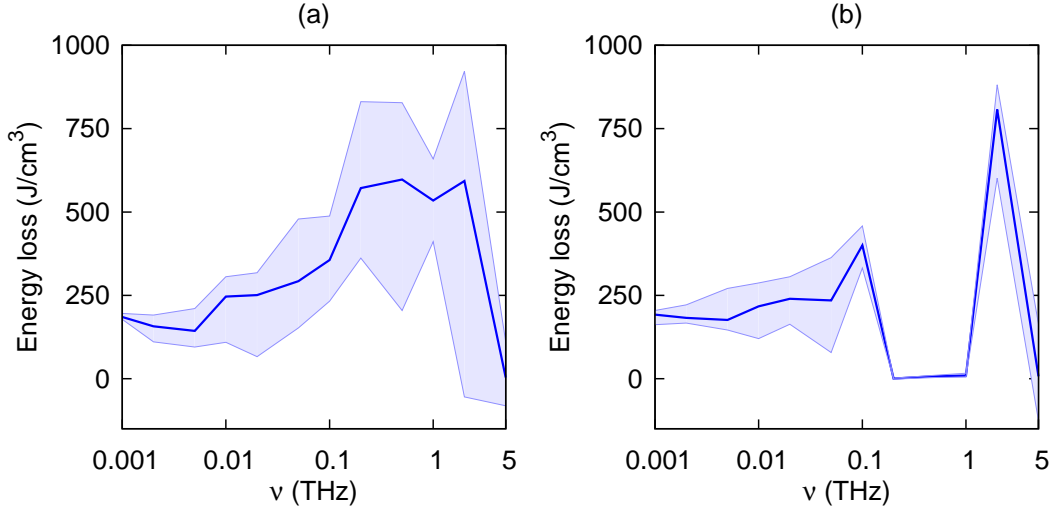


FIG. 4. Average energy loss per period for 11 (a) and 19 (b) unit cell thick films as a function of frequency. Shaded areas indicate largest deviation from the average.

## DYNAMICS OF AFE AND AFD ORDER PARAMETERS DURING THE PHASE SWITCHING AND POLARIZATION REVERSAL

To gain further insight into the intrinsic dynamics in  $\text{PbZrO}_3$  ultrathin films we analyze the time evolution of the polarization, AFE and AFD order parameters in 17 unit cell thick films subjected to the electric field with frequency of 0.01 THz. Fig. 5(b) and (c) give the time evolution of the polarization and the AFE order parameter, respectively, from 10th to 20th period of the electric field application. The areas shaded in blue indicate the time intervals when the film is mostly antipolar, whereas the areas with no shading indicate the time intervals when the film is mostly polar. Naturally, the polar phase is associated with the largest value of polarization, while the antipolar phase is associated with the largest value of the AFE order parameter. Schematic representation of the polar phase and associated polarization and AFD order parameter is given in Fig. 6(a). The antipolar phase and associated polarization and AFD order parameters are schematically represented in Fig. 6(b). We find all six possible  $\langle 110 \rangle$  directions for the AFE order

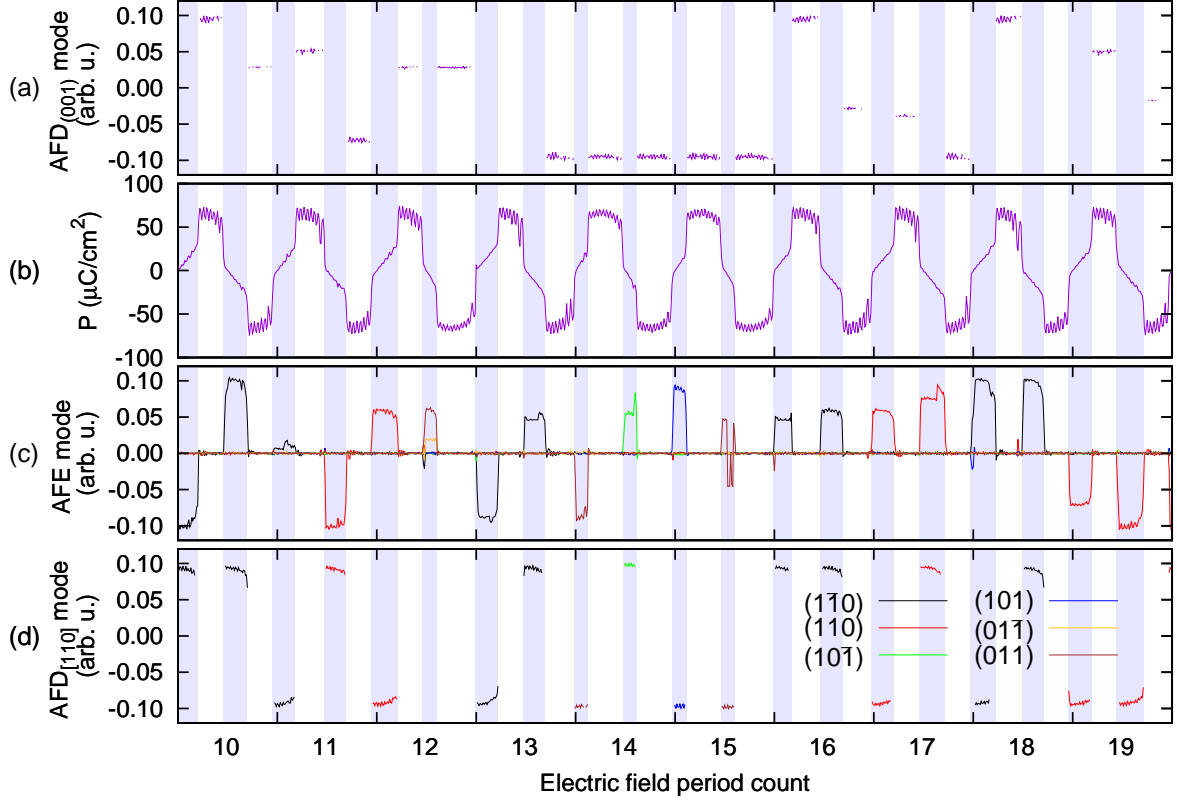


FIG. 5. The projection of the AFD order parameter onto the direction of the polarization vector during the time when the two are aligned within  $10^\circ$  of each other (a). Time evolution of the polarization (b) and the projections of the AFE order parameter (c). The direction for the projections are given in the legend. The projection of the AFD order parameter onto the direction of AFE order parameter during the time when the two are aligned within  $10^\circ$  of each other (d). Blue shading (no shading) indicates time intervals when the phase is mostly antipolar (polar). Data correspond to 17 unit cell thick film subjected to the ac electric field with the frequency of 0.01 THz.

parameter. Interestingly, however, the dynamics of the phase switching depends on the direction of the AFE order parameter. For example, the antipolar phase with in-plane direction of AFE order parameter is harder to switch into a polar phase as evident from the longer time interval associated with this phase. This is a strong indication that when AFE order parameter has an out-of-plane component, the antipolar phase is less stable under the electric field, as compared to the case when AFE order parameter lies in-plane. Moreover, the antipolar phase with the out-of-plane component of the AFE order parameter appears

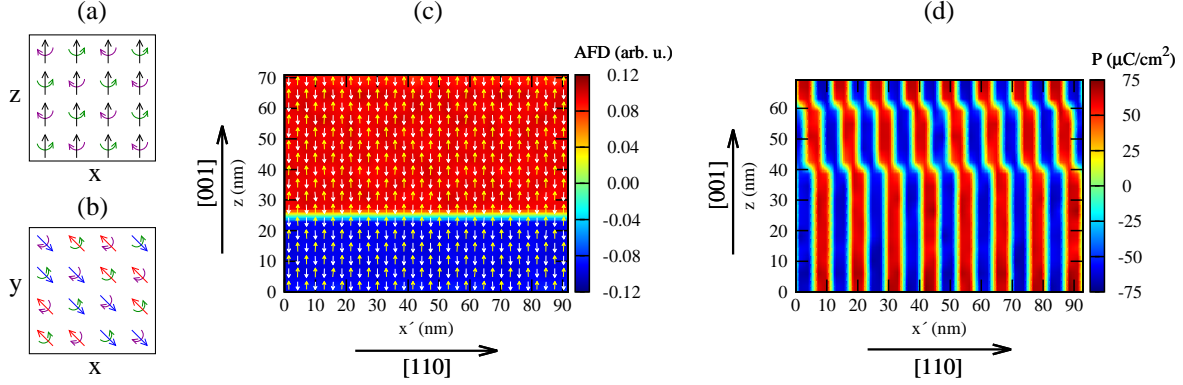


FIG. 6. (a) and (b) Schematic representation of the local dipole moments (black, red and blue arrows) and the sense of oxygen octahedra rotations (green and purple arrows) in the polar and antipolar phases, respectively. (c) Average local AFD order parameter in the  $(1\bar{1}0)$  plane of the film in the polar phase for  $t = 13.6T$  of the simulation presented in Fig. 5, where  $T$  is the electric field period. Color gives the projection of the local AFD order parameter onto  $[1\bar{1}0]$  direction. Arrows give the vectors describing local oxygen octahedra tilts [20]. (d) Average local polarization in  $(1\bar{1}0)$  plane of the film in the antipolar phase for time  $t = 12.8T$  of the same simulation. Color gives the projection of the local polarization onto  $[1\bar{1}0]$  direction.  $x'$  in panels (c) and (d) denotes the axis along  $[110]$  direction.

slightly less frequently in this simulations. For example, during the full simulation run of 30 periods the phase appears in 25 out of 60 occurrences of the antipolar phase. Once occurred it seems to appear over a few next periods, which suggests a memory effect. We find that similar to the case of  $\text{PbZrO}_3$  bulk the oxygen octahedra rotate about the direction of the local dipole moment (see schematization in Fig. 6(a) and (b)). This results in AFD order parameter aligning along the polar direction in the polar phase and antipolar direction in the antipolar phase. To illustrate that Fig. 5(a) reports the projection of the AFD order parameter onto the polarization direction for those times when AFD order parameter and the polarization are within  $10^\circ$  angle. The comparison of Fig. 5(a) and (b) indicates that in the polar phase the two order parameters indeed prefer to align with each other. We also notice that the polarization magnitude reaches its maximum value in each period of oscillations, while the AFD order parameter does not, which suggests formations of AFD domains. Example of such AFD domains is given in Fig. 6(c). It further suggests that formation of the polar phase is driven by the polar distortions, while AFD rotations just

follow at the local level which results in the formation of AFD domains. To establish the alignment of the order parameters in the antipolar phase we turn to Fig. 5(c) and (d). Figure 5(d) gives the projection of the AFD order parameter onto the direction of the AFE vector when the two order parameters are within  $10^\circ$  of each other. Comparison of Fig. 5(c) and (d) indicates that in the antipolar phase the two order parameters are mostly aligned with each other. In the antipolar phase we find that the magnitude of the AFD order parameter reaches its nearly maximum value in each period while the AFE order parameter does not. This suggests formation of nonequilibrium phases with AFE domains. Example of such AFE domains is given in Fig. 6(d). It further suggests that the formation of the antipolar phase is driven by the AFD motion while the antipolar distortions vector follows it, which results in formation of AFE domains.

To find out whether the polar and antipolar phases can coexist under nonequilibrium conditions we plot the polarization against the AFE order parameter in Fig. 7. In the ideal case when the order parameters do not coexist the data points would segregate around the the green crosses on the coordinate axes. In our case we find many data points off coordinate axes which reveals the coexistence of the order parameters under the nonequilibrium conditions. For comparison, we included data from the simulations where the electric field was applied quasi-statically. Only one period of electric field was simulated. We can see that in the latter case the two order parameters prefer to avoid each other as much as possible since the data points cluster on the coordinate axes. Note, that points clusters located near the green crosses on the  $x$ -axis correspond to the case of homogeneous antipolar phase. The points clusters located closer to the origin correspond to the phases with AFE domains.

## **NANOSCOPIC MECHANISM OF ELECTRIC-FIELD-INDUCED PHASE SWITCHING**

To reveal the nanoscopic mechanism associated with the field-induced antipolar-polar-antipolar phase switching we follow the field evolution of the order parameters and dipoles configurations in 12 unit cell thick film subjected to the field of 0.01 THz frequency. Note, that while at equilibrium this film exhibits FE behavior, at the chosen frequency it exhibits AFE behavior for some periods of the electric field. We focus on these periods. There exist two possible scenarios depending on the direction of the AFE order parameter in the

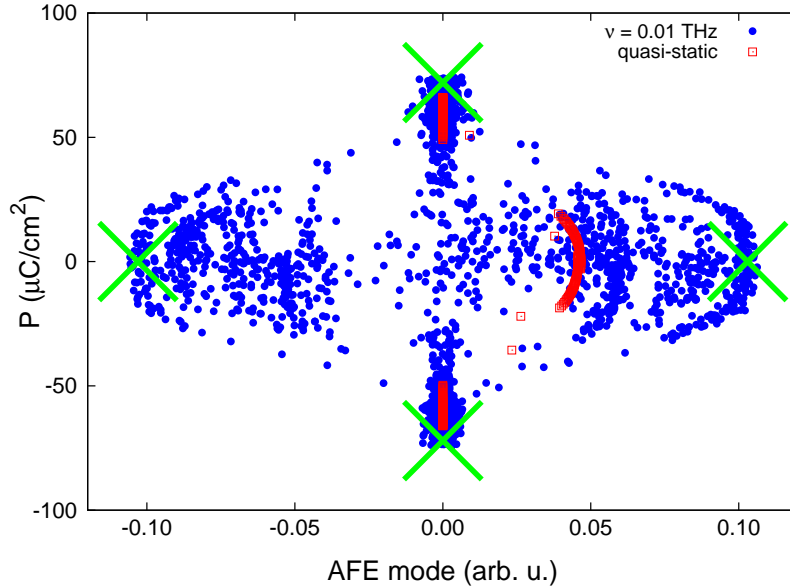


FIG. 7. Polarization vs AFE order parameter obtained from simulations in a 17 unit cell thick film subjected to the ac field with frequency of 0.01 THz (blue circles) and static field (red squares). Green crosses indicate the location of the points for the ideal case when the two order parameters do not coexist.

antipolar phase. *Scenario 1* occurs when initially the AFE order parameter is in-plane while the polar phase is induced along the out-of-plane direction. *Scenario 2* takes place when the AFE order parameter initially has an out-of-plane component while the polar phase is still induced along the out-of-plane direction.

*Scenario 1.* Fig. 8(a) shows the time evolution of the polarization and AFE order parameter during one period of the electric field associated with this Scenario. The evolution begins with a linear increase in polarization. Inspection of the dipoles patterns during this phase reveals that the polarization increases through rotation of the dipoles toward the out-of-plane direction, while still preserving the antipolar order. Indeed from Fig. 8 we find a finite AFE order parameter in this case. At  $t = 14$  ps the polarization starts increasing drastically and reaches its largest value at  $t = 16$  ps. During the same time interval the AFE order parameter decreases to zero. Microscopically, in this region the dipoles complete their rotation toward the out-of-plane direction. The process originates at the surfaces of the film and propagates inside. At  $t = 15$  ps the antipolar ordering inside the film coexists with the polar ordering in the vicinity of the surfaces. From 16 to 50 ps the film preserves the polar ordering. At  $t = 50$  ps both the polarization and AFE order parameters are zero indicating

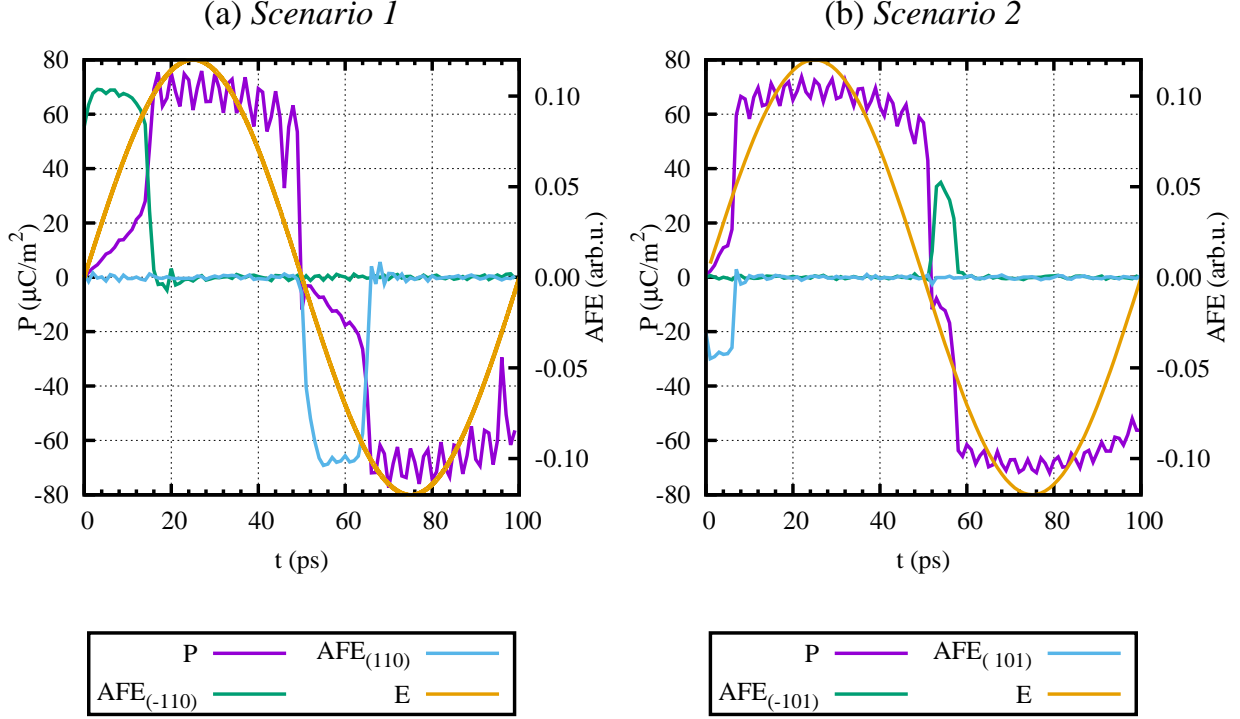


FIG. 8. Time evolution of the polarization, AFE order parameter and electric field in 12 unit cell thick film during one period of the electric field for *Scenario 1* (a) and *Scenario 2* (b). The subscript for AFE indicates the direction for the projection.

that the dipoles are completely disordered. This finding reveals that the polar-antipolar phase switching occurs via intermediate nonpolar phase.

As the electric field increases now in the opposite direction both the polarization and AFE order parameter grow in magnitude from  $t = 50$  to  $t = 55$  ps. In the beginning of this phase the nanostripes appear throughout the film, however, their ordering is somewhat short range. As the time progresses the nanostripes develop a long-range order that gives rise to the maximum value of the AFE order parameter at 55 ps. At the same time dipoles rotate toward the out-of-plane direction to follow the electric field. Once again we observe a moderate increase in polarization magnitude first followed by a drastic increase as the dipoles lose their in-plane components and AFE ordering. The polar phase establishes at  $t = 68$  ps.

Thus, our calculations reveal that in *Scenario 1* the field-induced antipolar-polar phase

switching occurs via two major phases. During the first longer phase the dipoles rotate towards the field, while preserving antipolar order for their in-plane components. During the second shorter phase the dipoles lose their in-plane components which leads to the disappearance of the antipolar ordering. The antipolar-polar phase transition is inhomogeneous and originates at the surfaces of the film, which favors the polar phase [5]. During this phase the regions of polar and antipolar phases coexist in the film. The field induced switching from polar to antipolar phase occurs in a qualitatively different way and is assisted by a formation of a nonpolar phase.

*Scenario 2.* We now describe the case when the AFE order parameter initially has an out-of-plane component. In particular, we consider the case when it is aligned along  $[-101]$  direction. In this case the dipoles in the stripes form the angles of  $45^\circ$  and  $135^\circ$  with the growth direction. The associated time evolution of the order parameters is given in Fig. 8(b). Under the electric field increasing in the positive  $z$ -direction the dipole evolution begins by rotation of dipoles in both types of stripes toward the direction of the electric field. This process is responsible for the initial growth of the polarization until 6.6 ps. The stripes with the  $z$ -component antiparallel to the field direction shrink to about one unit cell thickness. At 7.0 ps the stripes disappear entirely while the polarization continues to grow through further rotations of the dipoles toward the electric field. At 10 ps the dipoles are mostly aligned along the electric field. Unlike *Scenario 1* the antipolar-polar phase transition in this case is rather homogeneous throughout the thickness of the film. There is not much further change in the dipole configuration until 51 ps when the electric field, increasing in the opposite direction, forces dipoles to begin their rotations toward the electric field. Once again we find the formation of nonpolar phase first (at around 51 ps). Immediately after that the dipoles begin the direction reversal, however, encounter the antipolar phase and proceed with the stripes formation as evident from the growth of AFE order parameter and inspection of the dipole patterns. The stripe formation continues until 54 ps. However, the newly formed stripes are not perfect, so that the AFE order parameter is less than its equilibrium value. From 54 to 56 ps the polarization increases slightly along the field direction while AFE order parameter decreases as the AFE is destabilized by the field. At around 56 ps the polarization starts increasing dramatically along the field direction while the AFE order parameter vanishes. The polar phase is established at 58 ps.

Thus, we find that for both *Scenarios* the field-induced antipolar-polar phase transition

occurs through rotation of the dipoles toward the electric field, while polar-antipolar phase transition is assisted by formation of a nonpolar phase.

There are two interesting features to be noted from Fig. 8. Firstly, in agreement with the case of 17 unit cell thick film (see Fig. 5) we find that for *Scenario 2* the antipolar phase is easier to switch into a polar phase and harder to switch back from polar to antipolar phase as compared to the case of *Scenario 1*. Secondly, the average value of the polarization and its thermal oscillations in *Scenario 1* are slightly larger than in *Scenario 2*. To understand the origin of this we inspect the projections of the local dipole moments onto the growth direction,  $d_z$ . In the antipolar phase for *Scenario 2* the distribution for  $d_z$  is rather spread out centering around  $\pm d$  values, while for *Scenario 1* it is less spread out and centered around zero. As a result, in the nonequilibrium polar phase the distribution for  $d_z$  is also more spread out in case of *Scenario 2* than in case of *Scenario 1*. This leads to the presence of the two aforementioned features.

## CONCLUSIONS

To summarize we carried out detailed nanoscopic investigations of the phase switching and polarization reversal dynamics in ultrathin  $\text{PbZrO}_3$  films subjected to ac electric field with frequencies of 1 GHz and above. Our computational results led to the following insights.

(i) The intrinsic switching time for the phase transformation can be inferred from the deviations of the  $P(E)$  dependencies from their average values. We find that the intrinsic time for polar-antipolar and polar-polar phase switching is fraction of a nanosecond, while antipolar-polar phase switching is slightly slower (on the order of a nanosecond);

(ii) When the ac electric field amplitude is fixed to about 1.6 of the static coercive field the hysteresis loops undergo dramatic transformations as the frequency of the ac electric field frequency increases from 0.001 THz to 5 THz. Below 0.02 THz the evolution of the hysteresis loops is mostly set by the kinetics of the FE-AFE phase competition, while above this frequency the dynamics of the polar phonon starts playing an important role.

(iii) Application of high-frequency electric field leads to the formation of nonequilibrium phases that exhibit AFE and AFD nanodomains and coexistence of antipolar and polar order parameters that does not occur at equilibrium. However, even in such nonequilibrium phases the oxygen octahedra prefer to tilt about the direction of the (anti)polar vector.

(iv) At a nanoscopic level two *Scenarios* for the phase switching in ultrathin  $\text{PbZrO}_3$  films are possible depending on the direction of the AFE order parameter. When such order parameter has a component along the electric field direction the antipolar-polar phase switching occurs through the rotation of the dipoles toward the field and simultaneous shrinking of the domains with the unfavorable direction of the electric dipoles. On the other hand, when the AFE order parameter is perpendicular to the electric field, the antipolar-polar phase switching occurs through rotation of the dipoles toward the field followed by the formation of the polar phase near the film's surfaces. The polar domains propagate rapidly to the center of the film. In both *Scenarios* the polar-antipolar phase transition is assisted by the formation of a nonpolar phase. The kinetics of the phase switching is slightly different for these two *Scenarios*.

(v) As the film's thickness increases from 4.1 to 8.2 nm the dynamics of the phase switching and polarization reversal changes following the change in the electrical response of the film. In particular, for the films with FE behavior under quasi-static conditions (4.1 to 5.0 nm thickness) we find that as the frequency increases above 0.001 THz the films first begin to exhibit AFE phases in addition to the FE ones. As the frequency increases further and above 0.1 THz the dynamical response resembles the one of lossy dielectric. For the films with AFE behavior under quasi-static conditions (6.2 to 8.2 nm thickness) the dynamical response for the frequencies 0.001 to 0.01 THz is mostly determined by the intrinsic switching time between the FE and AFE phases. For the frequencies 1 THz and above the films exhibit mostly dielectric behavior. The films with "mixed" hysteresis loops under quasi-static conditions (5.0 to 6.2 nm thickness) exhibit features of both aforementioned cases.

## ACKNOWLEDGEMENTS

The present work is supported by the U.S. Department of Energy, Office of Basic Energy Sciences, Division of Materials Sciences and Engineering under grant DE-SC0005245. Computer time was provided by USF Research Computing, sponsored in part by NSF MRI CHE-1531590.

- 
- [1] C. W. Ahn, G. Amarsanaa, S. S. Won, S. A. Chae, D. S. Lee, and I. W. Kim, *ACS Appl. Mater. & Interfaces* **7**, 26381 (2015).
- [2] W. Geng, Y. Liu, X. Meng, L. Bellaiche, J. F. Scott, B. Dkhil, and A. Jiang, *Adv. Mater.* **27**, 3164.
- [3] E. Glazkova-Swedberg, J. Cuozzo, S. Lisenkov, and I. Ponomareva, *Comp. Mater. Sci.* **129**, 44 (2017).
- [4] X. Hao, J. Zhai, L. B. Kong, and Z. Xu, *Prog. Mater. Sci.* **63**, 1 (2014).
- [5] B. K. Mani, C.-M. Chang, S. Lisenkov, and I. Ponomareva, *Phys. Rev. Lett.* **115**, 097601 (2015).
- [6] B. K. Mani, R. Herchig, E. Glazkova, S. Lisenkov, and I. Ponomareva, *Nanotechnology* **27**, 195705 (2016).
- [7] G. Apachitei, J. J. P. Peters, A. M. Sanchez, D. J. Kim, and M. Alexe, *Adv. Elect. Mater.* **3**, 1700126.
- [8] D. Bao, R. Scholz, M. Alexe, and D. Hesse, *J. Appl. Phys.* **101**, 054118 (2007).
- [9] I. Kanno, S. Hayashi, R. Takayama, and T. Hirao, *Appl. Phys. Lett.* **68**, 328 (1996).
- [10] S.-E. Park, M.-J. Pan, K. Markowski, S. Yoshikawa, and L. E. Cross, *J. Appl. Phys.* **82**, 1798 (1997).
- [11] S. Ducharme, V. M. Fridkin, A. V. Bune, S. P. Palto, L. M. Blinov, N. N. Petukhova, and S. G. Yudin, *Phys. Rev. Lett.* **84**, 175 (2000).
- [12] G. Vizdrik, S. Ducharme, V. M. Fridkin, and S. G. Yudin, *Phys. Rev. B* **68**, 094113 (2003).
- [13] K. McCash, A. Srikanth, and I. Ponomareva, *Phys. Rev. B* **86**, 214108 (2012).
- [14] B. Y. Huang, Z. X. Lu, Y. Zhang, Y. L. Xie, M. Zeng, Z. B. Yan, and J.-M. Liu, *J. Appl. Phys.* **119**, 174103 (2016).
- [15] Y.-H. Kim and J.-J. Kim, *Phys. Rev. B* **55**, R11933 (1997).
- [16] X. Chen, F. Cao, H. Zhang, G. Yu, G. Wang, X. Dong, Y. Gu, H. He, Y. Liu, and G. L. Brenneka, *J. Am. Ceramic Soc.* **95**, 1163.
- [17] C. Liu, S. X. Lin, M. H. Qin, X. B. Lu, X. S. Gao, M. Zeng, Q. L. Li, and J.-M. Liu, *Appl. Phys. Lett.* **108**, 112903 (2016).
- [18] B. Xu, P. Moses, N. G. Pai, and L. E. Cross, *Appl. Phys. Lett.* **72**, 593 (1998).

- [19] R. Xu, Z. Xu, Y. Feng, X. Wei, J. Tian, and D. Huang, *Appl. Phys. Lett.* **109**, 032903 (2016).
- [20] B. K. Mani, S. Lisenkov, and I. Ponomareva, *Phys. Rev. B* **91**, 134112 (2015).
- [21] I. Ponomareva, I. I. Naumov, I. Kornev, H. Fu, and L. Bellaiche, *Phys. Rev. B* **72**, 140102 (2005).
- [22] D. Rapaport, *The Art of Molecular Dynamics Simulation* (Cambridge, 1997).
- [23] Z. G. Fthenakis and I. Ponomareva, *Phys. Rev. B* **96**, 184110 (2017).
- [24] J. Ge, Y. Chen, X. Dong, D. Rmiens, X. Guo, F. Cao, and G. Wang, *Thin Solid Films* **584**, 108 (2015).
- [25] A. Roy Chaudhuri, M. Arredondo, A. Hähnel, A. Morelli, M. Becker, M. Alexe, and I. Vrejoiu, *Phys. Rev. B* **84**, 054112 (2011).
- [26] A. K. Tagantsev, I. Stolichnov, N. Setter, J. S. Cross, and M. Tsukada, *Phys. Rev. B* **66**, 214109 (2002).